Effects of discreteness in the Green's function of a hyperbolic medium

Alena V. Shchelokova,[1] Alexander N. Poddubny,[1,2] and Pavel A. Belov[1]
[1]*ITMO University, St. Petersburg 197101, Russia*
[2]*Ioffe Physical-Technical Institute of the Russian Academy of Science, St. Petersburg 194021, Russia*
(Received 25 February 2014; published 26 August 2014)

We present a theoretical study of the discrete Green's function for the two-dimensional metamaterial, realized as a transmission line array. We demonstrate that the Green's function possesses distinct ripples when the isofrequency contour is of hyperbolic shape. This effect is a characteristic nonlocal feature of the hyperbolic regime and is beyond the effective medium approximation.

DOI: 10.1103/PhysRevA.90.023854 PACS number(s): 42.70.−a, 41.20.Jb, 78.67.Pt

I. INTRODUCTION

A hyperbolic medium is an electromagnetic medium, where the isofrequency curves for the plane-wave eigenmodes are of hyperbolic shape [1,2]. It is characterized by a permittivity tensor where the two principal components, e.g., ε_{xx} and $\varepsilon_{yy} = \varepsilon_{zz}$, are of the opposite sign. Thus, the hyperbolic medium is qualitatively different from a traditional uniaxial crystal, with elliptic isofrequency contours. The first realization of the hyperbolic regime was achieved for magnetized plasma in 1969 [3], when the characteristic conical antenna emission pattern was observed. Recently, hyperbolic media became a subject of active research in the field of artificial structured systems, metamaterials. Model systems for hyperbolic metamaterials include metallic multilayers [4], arrays of wires [5], and transmission line arrays [6,7]. Unusual hyperbolic dispersion leads to a huge number of potential applications for nanophotonics [4], sensing [8], heat transport [9], and field imaging and lensing [10]; see also the review in Ref. [2] and references therein.

Hyperbolic metamaterials are inherently discrete due to the finite size of their building blocks. Hence, a traditional effective medium description may fail to account for certain effects, and strong manifestations of nonlocality can be expected. Here, we study the Green's function, i.e., the distribution of the field, excited by a pointlike source in a hyperbolic medium. Knowledge of the Green's function is instrumental for calculation of arbitrary electromagnetic properties of the structure [11]. As an example, we choose the simplest nearest-neighbor two-dimensional tight-binding model of the hyperbolic metamaterial. This model is quite instructive and can be directly realized, e.g., in the two-dimensional transmission line structure [6,7,12,13], illustrated in Fig. 1. Such a structure is formed by coupled capacitors in one direction and coupled inductances in the perpendicular direction. The opposite sign of the impedances characterizing capacitors and inductances ensures the hyperbolic regime in the structure. Another possible realization could be based on the disk resonator structures where the local coupling is engineered by inserting bar links [14] or a coupled micropillar array [15]. We show that the field pattern has pronounced ripples, which are characteristic of the hyperbolic regime and cannot be described within the effective medium approximation.

II. MODEL

In this section we present the details for the Green's function calculation. We first discuss the effective medium limit and then proceed to the actual discrete model, corresponding to the transmission line metamaterial, shown in Fig. 1. In the continuum approximation of the two-dimensional hyperbolic medium the Green's function U_1 satisfies the two-dimensional scalar anisotropic Helmholtz equation, which can be presented as

$$\eta_x \frac{d^2U_1}{dx^2} + \eta_y \frac{d^2U_1}{dy^2} + U_1 = -\delta(x - x_0)\delta(y - y_0). \qquad (1)$$

Here, the constants η_x and η_y characterize the propagation of the waves in the two corresponding directions. In particular, for the electromagnetic transverse magnetic wave propagation along the z axis, the values of η_x and η_y are inversely proportional to the ε_{xx} and ε_{yy} components of the dielectric tensor. The singular term on the right-hand side of Eq. (1) describes the excitation in the point $x = x_0$, $y = y_0$. In order to facilitate the following discretization of Eq. (1), we have chosen the coordinates x and y to be dimensionless from the start. The spatial dependence of the plane-wave mode is then given by $\exp(ik_x xd + ik_y yd)$, where k_x and k_y are Cartesian components of the wave vector and d is the size of the transmission line unit cell. The isofrequency contour for Eq. (1) is determined from the equation

$$\eta_x(k_x d)^2 + \eta_y(k_y d)^2 = 1. \qquad (2)$$

When the constants η_x and η_y are positive, the wave propagation is allowed in both x and y directions and the contour is of elliptic shape. In the hyperbolic regime, when either η_x or η_y is negative, the propagation is possible only in one direction. In this case the spatial pattern of the Green's function

$$U_1(x,y) = \frac{i}{4} H_0^{(1)}\left[\sqrt{\frac{(x - x_0)^2}{\eta_x} + \frac{(y - y_0)^2}{\eta_y}}\right] \qquad (3)$$

of Eq. (1) has a characteristic hourglass shape [3,16,17]. Our goal is to go beyond the continuous approximation of Eq. (1) and examine the effects of the medium discreteness on the Green's function pattern.

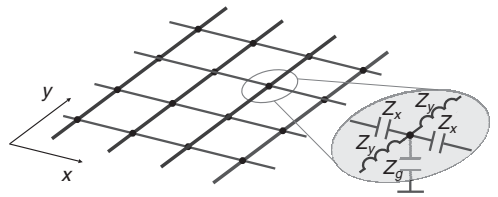

FIG. 1. Schematic illustration of the hyperbolic metamaterial based on a transmission line. The inset shows the unit cell with inductances and capacitances.

To this end, we consider the scalar two-dimensional discrete model,

$$\eta_x(U_{x-1,y} + U_{x+1,y} - 2U_{x,y}) + \eta_y(U_{x,y-1} + U_{x,y+1} - 2U_{x,y}) + U_{x,y} = -\delta_{x,x_0}\delta_{y,y_0}, \tag{4}$$

where the derivatives in Eq. (1) have been replaced by the finite differences and the quantities x and y now label the unit cell numbers. On the one hand, this is a very simple nearest-neighbor tight-binding [18] model which allows efficient numerical and analytical solution. On the other hand, it can be directly realized in the transmission line metamaterial [7,12,13]. In this case Eq. (4) has the meaning of a Kirchhoff equation, with $U_{x,y}$ being the voltage in the node (x,y); $\eta_x = -Z_g/Z_x$ and $\eta_y = -Z_g/Z_y$, where Z_g is the ground impedance and $Z_{x,y}$ are the impedances, describing inductors and capacitors for the corresponding directions. The dispersion equation for the Bloch solution of Eq. (4) reads

$$\eta_x \sin^2\frac{k_x d}{2} + \eta_y \sin^2\frac{k_y d}{2} = \frac{1}{4} \tag{5}$$

and reduces to Eq. (2) in the long-wavelength limit $kd \ll 1$.

III. RESULTS AND DISCUSSION

Now we present the results of numerical solution of Eq. (4) in elliptic and hyperbolic regimes. Figure 2 shows the spatial pattern of the Green's function [Fig. 2(a)] and the isofrequency contour [Fig. 2(b)] calculated for the structure in the elliptic regime with $\eta_x = 28$, $\eta_y = 31$. The simulation was run for a finite square 51×51 grid with the source in the middle ($x_0 = y_0 = 26$). At the edges, the structure was loaded by the resistors with $R = 100\ \Omega$ to provide the boundary matching conditions. The pattern in Fig. 2 is mostly homogenous. Due to the finite-size effects, the pattern has a fourfold rotation symmetry with maxima near the corners of the square, rather than the circular symmetry. No specific features of discreteness are manifested in Fig. 2. We proceed to the hyperbolic regime. Figure 3(a) shows the pattern, calculated for $\eta_x = -1.1$, $\eta_y = 1.9$. The corresponding isofrequency contour is presented in Fig. 3(b). The figure demonstrates that the spatial distribution of the Green's function is significantly more complex than that in the elliptic regime; cf. Figs. 3(a) and 2(a). The distribution has an hourglass-like shape and it is concentrated within the polar angles

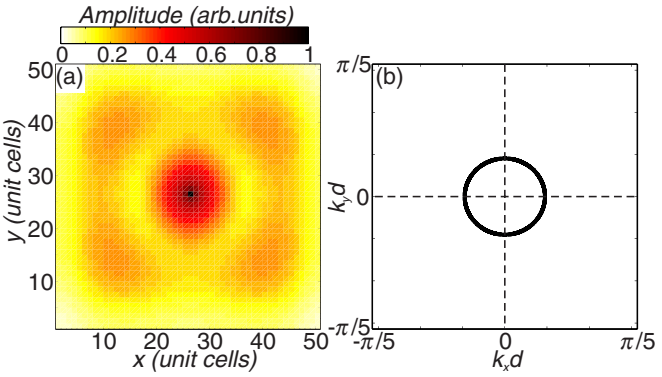

FIG. 2. (Color online) (a) The simulated spatial distribution of the absolute values of the Green's function in the two-dimensional elliptic medium with $\eta_x = 28$, $\eta_y = 31$. (b) Isofrequency curves obtained by numerical solution of the dispersion relation Eq. (5). The calculation has been performed for $x_0 = y_0 = 26$, and the structure included 51×51 unit cells.

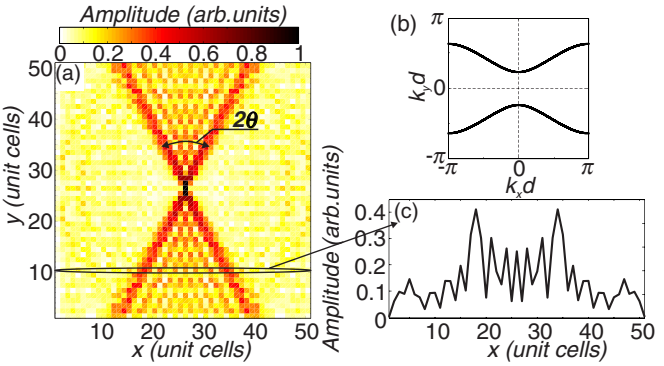

FIG. 3. (Color online) The simulated spatial distribution of the absolute values of the Green's function in the two-dimensional hyperbolic medium with $\eta_x = -1.1$, $\eta_y = 1.9$. (b) Isofrequency curves obtained by numerical solution of the dispersion relation Eq. (5).

$$|\theta| < \theta_0, \quad |\pi - \theta| < \theta_0, \quad \theta_0 = \arctan\sqrt{|\eta_x/\eta_y|}, \tag{6}$$

corresponding to the propagating waves [here $\tan\theta \equiv (x - x_0)/(y - y_0)$]. In the infinite structure the Green's function values outside the region of Eq. (6) are exponentially small. For the considered finite-size system the reflection at the top edges allows the penetration of the waves outside the hourglass region; see Fig. 3(a). Propagation and reflection of the waves, emitted from the small source in the hyperbolic medium, were studied both theoretically and experimentally [6]. Here, we focus on another effect, manifested in Fig. 3(a): the periodic ripples, which exist inside the propagating waves region in Eq. (6). These ripples are clearly manifested as a checkerboard pattern in Fig. 3(a). To visualize them better, we have plotted in Fig. 3(c) the pattern cross section, namely, the absolute values of the Green's function $|U(x,y)|$ as functions of x at given y. The ripples correspond to the rapid oscillations in the central part of Fig. 3(c) with the period close to 2. We stress that Fig. 3 presents the absolute values of the Green's function, and not the real part. Hence, the ripples are not related to the periodic phase profile of the emitted waves.

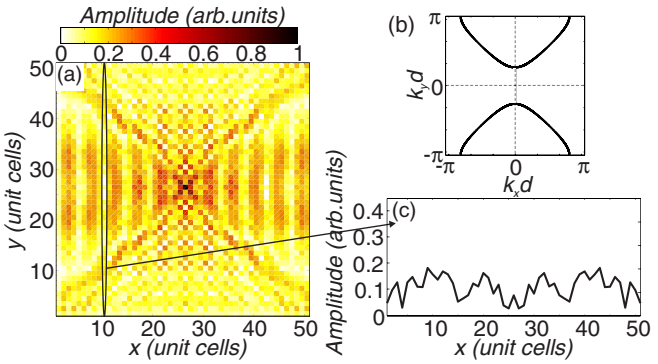

FIG. 4. (Color online) (a) The simulated spatial distribution of the Green's function absolute values in the two-dimensional hyperbolic medium with $\eta_x = -1.5$, $\eta_y = 1.5$. (b) Isofrequency curves obtained by numerical solution of the dispersion relation Eq. (5). (c) The absolute values of the Green's function at the fixed coordinate $y = 10$.

Figure 4 presents the same results as Fig. 3, but for $\eta_x = -1.5$, $\eta_y = 1.5$. Counterintuitively, the checkerboard ripples pattern is absent in this case, although the overall hourglass Green's function structure is not dramatically changed. Close comparison of Figs. 3 and 4 reveals the difference between the isofrequency contours in these regimes. In the case of Fig. 3(c), the isofrequency curves end at the left and right edges of the Brillouin zone, where $|k_y| = \pi/d$. In the case of Fig. 4(c), these curves end at the top and bottom Brillouin zone edges, where $|k_x| = \pi/d$. The type of termination of the isofrequency curves depends on the ratio between the propagation constants η_x and η_y, determining the angle θ_0 in Eq. (6). For $|\eta_x| < |\eta_y|$ one has $\theta_0 < \pi/4$ and the termination of type Fig. 3(b); the case when $|\eta_x| \gtrsim |\eta_y|$ corresponds to $\theta_0 \gtrsim \pi/4$ results in the termination of type Fig. 4(c).

The presence of ripples in Figs. 3 and 4 is an effect of discreteness, which is beyond the effective medium approximation Eq. (3). We have numerically checked that the ripples pattern depends only on the ratio $|\eta_x|/|\eta_y|$ and is not qualitatively sensitive to the structure size. In order to provide conclusive evidence that the ripples are due to the specific termination of the isofrequency curves, we present in Fig. 5 the semianalytical results for the Green's function pattern. To this end, we seek the solution of Eq. (4) in infinite structure as a plane-wave expansion, which results in

$$U_2(x,y) = -\iint_{\substack{|k_x|<\pi/d \\ |k_y|<\pi/d}} \frac{d^2k}{(2\pi)^2} \times \frac{e^{ik_x d(x-x_0)+ik_y d(y-y_0)}}{2\eta_x(\cos k_x d - 1) + 2\eta_y(\cos k_y d - 1) + 1}. \quad (7)$$

Here, the integration is performed over the wave vectors lying inside the Brillouin zone of the square lattice. The structure of Eq. (7) is typical for the Green's function: the integral has poles at the wave vectors, corresponding to the system eigenmodes [19–21]. Contrary to the numerical solution of Eq. (4), the expression in Eq. (7) does not include any finite-size effects. However, it still accounts for the discreteness of the system because of the finite wave vector cutoff. Figure 5(a) shows the Green's function pattern plotted after Eq. (7). It looks very similar to the direct numerical solution in Fig. 3(a) and also has the ripples. This proves that the ripples are a size-independent feature.

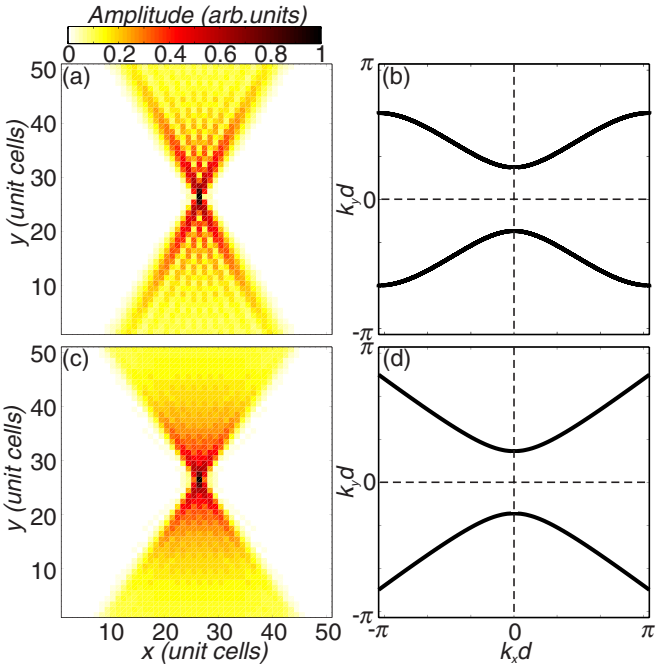

FIG. 5. (Color online) (a) The spatial distribution of the Green function absolute values in the two-dimensional hyperbolic medium obtained after Eq. (7). (b) Isofrequency curves obtained by numerical solution of the dispersion relation Eq. (5). (c) Approximate spatial distribution of the Green function absolute values in the two-dimensional hyperbolic medium obtained after Eq. (8). (d) Approximate isofrequency curves obtained from the continuous-limit dispersion relation Eq. (2). Calculation parameters are the same as in Fig. 3.

Now we simplify Eq. (7) by replacing the cosine functions in the denominator by their Taylor expansions in the long-wavelength limit, $|kd| \ll 1$:

$$U_3(x,y) = \iint_{\substack{|k_x|<\pi/d \\ |k_y|<\pi/d}} \frac{d^2k}{(2\pi)^2} \frac{e^{ik_x d(x-x_0)+ik_y d(y-y_0)}}{\eta_x(k_x d)^2 + \eta_y(k_y d)^2 - 1}. \quad (8)$$

The corresponding Green's function pattern is shown in Fig. 5(c) and completely lacks the ripples. Hence, the presence of the ripples is due to the difference between the denominators of Eqs. (7) and (8). The vanishing denominator of Eq. (8) corresponds to the approximate dispersion Eq. (5) [Fig. 5(d)], where the isofrequency curves are terminated at sharp angles to the Brillouin zone edge. Equation (7) corresponds to the exact isofrequency contour Eq. (5) [Fig. 5(b)], where the curves are terminated at right angles to the Brillouin zone edge. Such termination leads to the extra density of plane waves with the wave vectors at the Brillouin zone edge. It is the interference between these waves that explains the rippling of the Green's function pattern. An analogous effect has been recently predicted for three-dimensional hyperbolic metamaterial made of discrete dipoles [20]. It has been

interpreted as a manifestation of the Van Hove singularities in the Green's function [18,22]. However, the pattern of the ripples was completely different due to the metamaterial model. In particular, the considered structure is two-dimensional and includes only nearest-neighbor interactions, contrary to Ref. [20]. Nevertheless, the presence of the ripples is a quite general property of the hyperbolic metamaterials due to the isofrequency curve termination at the Brillouin zone edge.

IV. SUMMARY

To summarize, we have analyzed the spatial distribution of the Green's function for two-dimensional metamaterials. It has been demonstrated that the Green's function pattern has peculiar checkerboard ripples when the structure is in the hyperbolic regime. Moreover, the ripples are present in the hyperbolic regime only when the angle θ_0, characterizing the angular width of the hourglass Green's function pattern, is smaller than $\pi/4$. This corresponds to the following relation between the propagation constants in x and y directions: $-\eta_x < \eta_y$ (if $\eta_x < 0$ and $\eta_y > 0$), or $-\varepsilon_{xx} < \varepsilon_{yy}$. The ripples are the manifestation of the structure discreteness and cannot be described within the effective medium approximation. In particular, they arise due to the specific termination of the hyperbolic isofrequency curves at the Brillouin zone edge with $k_x = \pm\pi/d$ and are absent when the curves terminate at $k_y = \pm\pi/d$.

This effect demonstrates an importance of the nonlocality and discreteness features for hyperbolic metamaterials and is to be accounted for in the design of future metadevices. Our results are directly applicable to the transmission line arrays and can be straightforwardly generalized to any two-dimensional metamaterial structure composed of discrete elements with nearest-neighbor coupling.

ACKNOWLEDGMENTS

This work was supported by the Government of the Russian Federation (Grant No. 074-U01), the Ministry of Education and Science of the Russian Federation (Grant No. 11.G34.31.0020, Zadanie No. 3.1231.2014/K, Zadanie No. 3.561.2014/K), the Russian Foundation for Basic Research (Grant No. 14-02-92604), and the Dynasty Foundation (Russia). A.V.S. acknowledges support of an SPIE Optics and Photonics Education Scholarship.

[1] M. Noginov, M. Lapine, V. Podolskiy, and Y. Kivshar, Opt. Express **21**, 14895 (2013).
[2] A. Poddubny, I. Iorsh, P. Belov, and Y. Kivshar, Nat. Photonics **7**, 948 (2013).
[3] R. K. Fisher and R. W. Gould, Phys. Rev. Lett. **22**, 1093 (1969).
[4] H. N. S. Krishnamoorthy, Z. Jacob, E. Narimanov, I. Kretzschmar, and V. M. Menon, Science **336**, 205 (2012).
[5] J. Yao, Z. Liu, Y. Liu, Y. Wang, C. Sun, G. Bartal, A. M. Stacy, and X. Zhang, Science **321**, 930 (2008).
[6] K. Balmain, A. Luttgen, and P. Kremer, Antennas Wireless Propag. Lett. **1**, 146 (2002).
[7] A. V. Chshelokova, P. V. Kapitanova, A. N. Poddubny, D. S. Filonov, A. P. Slobozhanyuk, Y. S. Kivshar, and P. A. Belov, J. Appl. Phys. **112**, 073116 (2012).
[8] A. V. Kabashin, P. Evans, S. Pastkovsky, W. Hendren, G. A. Wurtz, R. Atkinson, R. Pollard, V. A. Podolskiy, and A. V. Zayats, Nat. Mater. **8**, 867 (2009).
[9] Y. Guo, C. L. Cortes, S. Molesky, and Z. Jacob, Appl. Phys. Lett. **101**, 131106 (2012).
[10] Z. Liu, H. Lee, Y. Xiong, C. Sun, and X. Zhang, Science **315**, 1686 (2007).
[11] L. Novotny and B. Hecht, *Principles of Nano-Optics* (Cambridge University Press, New York, 2006).
[12] A. Grbic and G. Eleftheriades, IEEE Trans. Antennas Propag. **51**, 2604 (2003).
[13] A. Grbic and G. V. Eleftheriades, J. Appl. Phys. **98**, 043106 (2005).
[14] Y. Nakata, T. Okada, T. Nakanishi, and M. Kitano, Phys. Rev. B **85**, 205128 (2012).
[15] T. Jacqmin, I. Carusotto, I. Sagnes, M. Abbarchi, D. D. Solnyshkov, G. Malpuech, E. Galopin, A. Lemaître, J. Bloch, and A. Amo, Phys. Rev. Lett. **112**, 116402 (2014).
[16] L. Felsen and N. Marcuvitz, *Radiation and Scattering of Waves* (Wiley-Interscience, New York, 2003).
[17] A. S. Potemkin, A. N. Poddubny, P. A. Belov, and Y. S. Kivshar, Phys. Rev. A **86**, 023848 (2012).
[18] C. Kittel, *Introduction to Solid State Phys.* (Wiley, New York, 1996).
[19] M. Born and E. Wolf, *Principles of Optics* (Pergamon Press, New York, 1970).
[20] A. N. Poddubny, P. A. Belov, P. Ginzburg, A. V. Zayats, and Y. S. Kivshar, Phys. Rev. B **86**, 035148 (2012).
[21] A. N. Poddubny, P. A. Belov, and Y. S. Kivshar, Phys. Rev. B **87**, 035136 (2013).
[22] R. H. Swendsen and H. Callen, Phys. Rev. B **6**, 2860 (1972).